Surfaces of Rod Photoreceptor Disk Membranes: Integral Membrane Components

DOROTHY J. ROOF and JOHN E. HEUSER

Department of Biochemistry and Biophysics, University of California School of Medicine, San Francisco, California 94143; and Department of Physiology and Biophysics, Washington University School of Medicine, St. Louis, Missouri 63110. Dr. Roof's present address is the Department of Biological Sciences, Purdue University, West Lafayette, Indiana 47907.

ABSTRACT The membrane surfaces within the rod outer segment of the toad, *Bufo marinus*, were exposed by rapid-freezing followed by freeze-fracture and deep-etching. Platinum-carbon replicas of disk membranes prepared in this way demonstrate a distinct sidedness. The membrane surface that faces the lumen of the disk shows a fine granularity; particles of ~6 nm are packed at a density of ~30,000/μm^2. These dimensions suggest that the particles represent protrusions of the integral membrane protein, rhodopsin, into the intradisk space. In addition, when rhodopsin packing is intentionally perturbed by exhaustive digestion with phospholipase C, a concomitant change is observed in the appearance of the luminal surface granularity. The cytoplasmic surface of the disk rarely displays this rough texture; instead it exhibits a collection of much larger particles (8–12 nm) present at ~10% of the concentration of rhodopsin. This is about the size and concentration expected for certain light-regulated enzymes, cGMP phosphodiesterase and GTP-binding protein, which are currently thought to localize on or near the cytoplasmic surface of the disk. The molecular identity of the 8–12-nm particles will be identified in the following companion paper. A further differentiation of the cytoplasmic surface can be seen around the very edge, or rim, of each disk. This rim has relatively few 8–12-nm particles and instead displays short filamentlike structures connecting it to other membranes. These filaments extend between adjacent disks, across disk incisures, and from disk rims to the nearby plasma membrane.

The outer segment of the rod photoreceptor cell accomplishes the process of phototransduction by receiving a photon signal and converting it into an electrical signal. In rods, the site of photon absorption, the disk membrane, is osmotically (22) and electrically (16) separated from the site at which the first electrical response is generated, the plasma membrane. Two types of theories exist to explain how the absorption of a photon by rhodopsin in the disk membrane triggers an electrical response in the plasma membrane, which can be up to 2 to 3 μm distant in amphibian rods. Although both ideas postulate an "internal transmitter," the first emphasizes the compartmentalizing nature of the disk. According to this idea, a transmitter stored within the disk is released from that compartment by light and diffuses to sodium channels in the plasma membrane, closing them and hyperpolarizing the cell. An example of this model for transduction is the "calcium hypothesis" originally proposed by Yoshikami and Hagins (49), in which calcium is the internal transmitter.

An alternative view emphasizes the role of the disk surface as the site of transduction without invoking transport of any kind across the disk membrane. In such a model, calcium might be released from binding sites at the surface of the disk and diffuse to the plasma membrane as suggested above. Alternatively, a transmitter could actually be generated at the disk surface. According to one idea, the "cyclic nucleotide hypothesis" (5, 27, 48), the disk membrane would simply act as an anchor for the light-absorbing molecule, rhodopsin. Upon exposure to light, rhodopsin could activate critical enzymes also located on the disk membrane. The cyclic nucleotide hypothesis suggests that these critical enzymes are a light activated cGMP phosphodiesterase (PDE) and a light activated regulatory GTP-binding protein (GBP). A light-induced drop in cGMP concentration in the interdisk space could subsequently alter sodium conductance of the plasma membrane, either directly or indirectly via a cascade of phosphorylation reactions. The evidence in favor of both types of hypothesis has been reviewed recently with no definite choice yet possible (20, 34).

THE JOURNAL OF CELL BIOLOGY · VOLUME 95 NOVEMBER 1982 487–500
© The Rockefeller University Press · 0021-9525/82/10/0487/14 $1.00

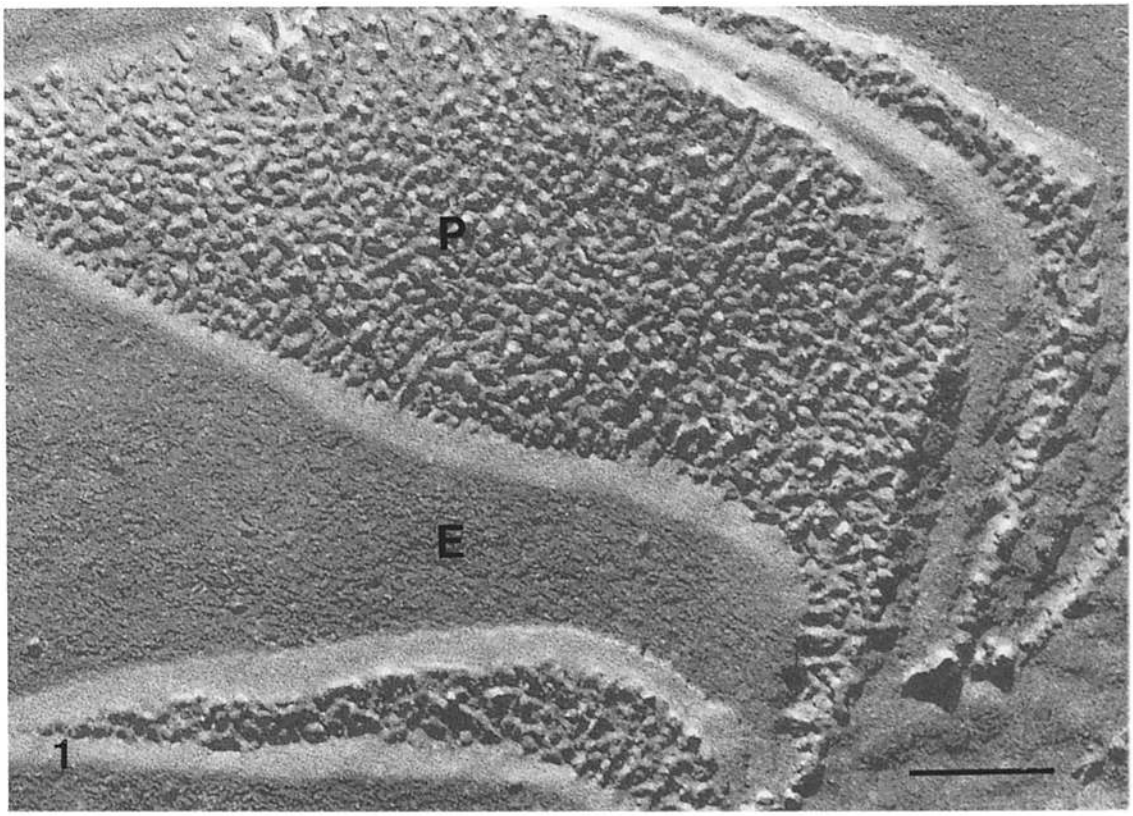

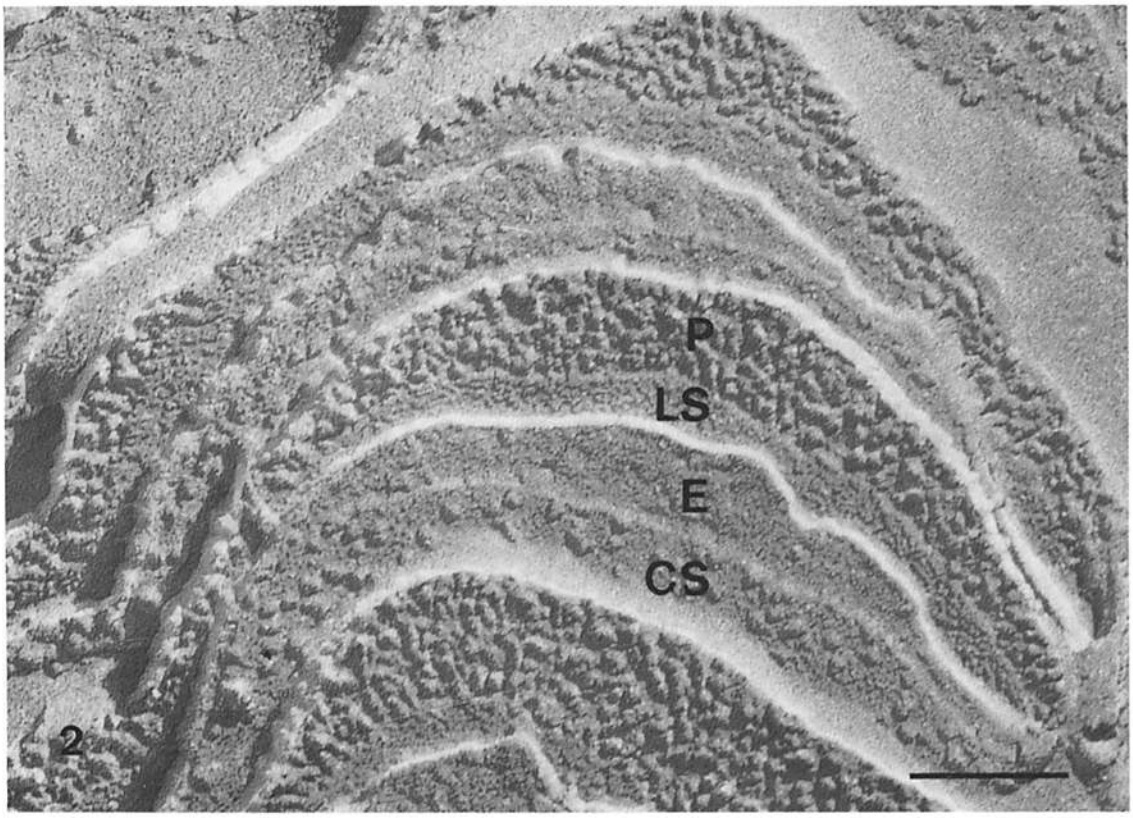

FIGURES 1 and 2 Fig. 1: Fragmented, swollen toad ROS which was rapidly frozen, fractured at −110°C, and unidirectionally shadowed with Pt/C at a 45° angle. The two fracture faces, *E* and *P*, are separated by large steps due to intentional swelling of the ROS before freezing. Bar, 0.1 μm. × 190,000. Fig. 2: Toad ROS prepared as in Fig. 1 and etched for 30 s at −95°C before unidirectional shadowing at a 45° angle. The P and E fracture faces are similar to those in Fig. 1. Interposed between the P and E faces are two additional surfaces exposed by brief etching. Each new surface is distinct. *LS*, the luminal surface of the disk membrane, is covered by a fine granularity. *CS*, the cytoplasmic surface of the disk membrane, shows a scattering of 8–12 nm large particles. Bar, 0.1 μm. × 210,000.

The final decision about which hypothesis most adequately explains transduction may require a careful sorting out of the molecules involved. This approach is particularly difficult in the case of interfacial events because of the complex interaction of molecules both at the surface of the membrane and, simultaneously, with other molecules in solution. It is already clear that there are several components involved in regulation of cyclic nucleotides, some of which are integral membrane proteins, some of which are only weakly bound to the membrane, and some of which are soluble factors (42) (see reference 24 for a review). Preliminary evidence indicates that many of these components are confined to the cytoplasmic surface (CS) of the disk membrane and form transient complexes in the plane of the membrane (27, 41). In addition, some peripheral proteins may fulfill their regulatory function by coming on and off the membrane (23–25). Clearly, the dynamic features of these interfacial events would have to be studied on a timescale of milliseconds in order to determine their role in phototransduction.

Several groups are attempting to purify and characterize all of the major proteins in the rod outer segment (ROS) (3, 4, 14, 15, 23, 24, 30). An alternative approach to these problems in "microtopography" would be to examine the surface of photoreceptor membranes, attempt to identify the molecules present there, and finally, to assemble a rapid time-sequence of changes in these molecules upon presentation of a bleaching flash.

We attempted to develop such an approach using quick-freeze, freeze-fracture, and deep-etch techniques (19). Here we describe integral components associated with disk membranes which may be related to the maintenance of shape and structure of the rod outer segment. Attempts are made to identify some of these components and infer their physiological role. Our following companion paper treats peripheral proteins of the disk membrane in a similar manner by identifying features on the CS of the disk and determining their contributions to the physiology of the rod photoreceptor. These results have been previously presented in preliminary form (38, 39).

MATERIALS AND METHODS

Tissue Preparation

Toads, *Bufo marinus*, (William Lemberger Assoc., Germantown, WI), were kept from one to several weeks in a large tank with running warm water under 12-h cycles of light and darkness. The animals were fed live crickets *ad lib.* once or twice weekly. Before dissection, toads were dark adapted for at least 12 h and were then decapitated and pithed either in total darkness or under dim red light. Dissections and all manipulations were performed at room temperature and under infrared illumination with the aid of an image converter (Electrophysics Corp., Nutley, NJ). Eyes were removed and bisected with a razor blade. The posterior half of the eye was cut into thirds and these pieces were placed in a modified isoosmotic Ringer's solution (110 mM NaCl, 2.5 mM KCl, 1 mM $CaCl_2$, 2 mM $MgCl_2$, 10 mM HEPES, pH 7.4). The retina was then gently teased out. For experiments with intact retinas, the pieces of retina were held at room temperature in oxygen-saturated Ringer's solution until rapid-freezing (usually <1 h). For experiments in which the outer segments were isolated and disk membranes exposed, the pieces of retina were trimmed free of any pigment epithelium and incubated (0.6 ml/retina) in a solution approximately one-tenth of the osmotic pressure of the normal Ringer's solution but with the normal complement of divalent ions (11 mM NaCl, 0.25 mM KCl, 1 mM $CaCl_2$, 2 mM $MgCl_2$, 10 mM HEPES, pH 7.4). The pieces of retina remained in the hypoosmotic solution for 1 to 2 min and the suspension was then swirled very gently. The pieces of retina were then removed from the suspension and discarded. The suspension containing the ROS fragments was gravity filtered through a wire mesh and subsequently kept at 4°C. The ROS fragments were collected by centrifugation at 9,000 *g* at 4°C and were resuspended in small volumes (50–100 μl) for rapid-freezing. These aliquots were held at 4°C for up to 1 h and were warmed to room temperature immediately before rapid-freezing. Absorption spectra of these aliquots dissolved in 1% Ammonyx LO (Onyx Chemical Co., Jersey City, NJ) exhibited $A_{280/498}$ in the range of 2.7–3.0 and $A_{400/498}$ in the range of 0.34–0.37.

For experiments with rat or cattle retinas, the retinas were handled as described above substituting mammalian isoosmotic Ringer's (130 mM NaCl, 3.5 mM KCl, 2 mM $MgCl_2$, 2 mM $CaCl_2$, 10 mM HEPES, pH 7.4) during dissection and approximately one-tenth isoosmotic mammalian Ringer's with normal divalent ion complement to prepare ROS fragments. Rats were 250–300 g female Sprague-Dawley albinos (Simonsen Laboratories, Gilroy, CA) and cattle eyes were obtained fresh (McDermott Meat Packing Co., Berkeley, CA).

The experiments with ROS fragments were repeated using TRIS Ringer's (10 mM TRIS substituted for 10 mM HEPES) with no apparent effect on the features observed. Because of the difficulty of operating the rapid-freezing equipment in total darkness, all tissues were exposed to fluorescent room light for several minutes before rapid-freezing, except where indicated in the text.

Phospholipase C Digestion

Outer segment fragments prepared as described above were suspended in 100 μl/retina of 100 mM TRIS maleate, 1 mM $ZnCl_2$, pH 7.0. Phospholipase C (Boehringer Mannheim Biochemicals, Indianapolis, IN), dialyzed against 100 mM TRIS maleate, 1 mM $ZnCl_2$, pH 7.0, was added to a final concentration of 0.5 U/nmol rhodopsin. The suspension was gently stirred at room temperature for 1 h and the reaction was stopped by pelleting at 9,000 *g* and washing the membranes twice with calcium/magnesium free 0.1 isoosmotic Ringer's plus 2 mM EDTA. The membranes were collected by centrifuging at 9,000 *g* and resuspended in a small volume of 0.1 isoosmotic Ringer's for rapid-freezing. The digestion procedure was carried out under dim red light.

Quick-freezing

Small pieces of the unfixed retina were supported on 3-×-3-×-0.8-mm cushions of rat lung and were mounted in the rapid-freezing device previously described

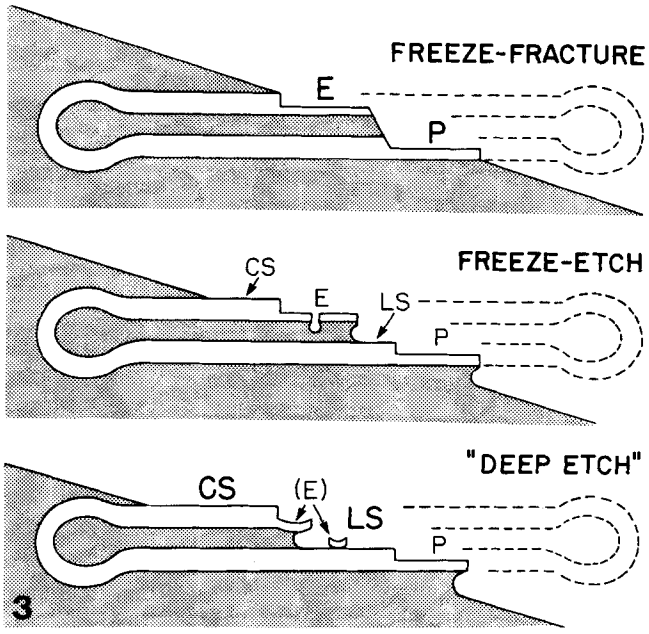

FIGURE 3 Diagram of the effects of increasing amounts of etching on a single disk from fragmented, swollen ROS. Freeze-fracture exposes only two faces, one smooth (*E*) and one roughly "cobblestoned" (*P*). Compare with Fig. 1. Freeze-etch represents brief (30 s) etching at −95°C after freeze-fracture. Two additional faces, *LS* and *CS*, are exposed. *LS* shows a fine 6-nm granularity. In contrast, *CS* shows a collection of large (8–12 nm) particles. As previously observed by others, brief etching also causes depression or pits to form in the otherwise smooth E fracture face. Compare this diagram with Figs. 2 and 4. Deep-etch: after prolonged (3 min) etching at −95°C, the E fracture face pits have enlarged, apparently merging in some places. Small fragments of the E fracture face are deposited onto the underlying luminal surface of the disk membrane. This E face debris can be clearly seen overlying the finely textured LS in Figure 5.

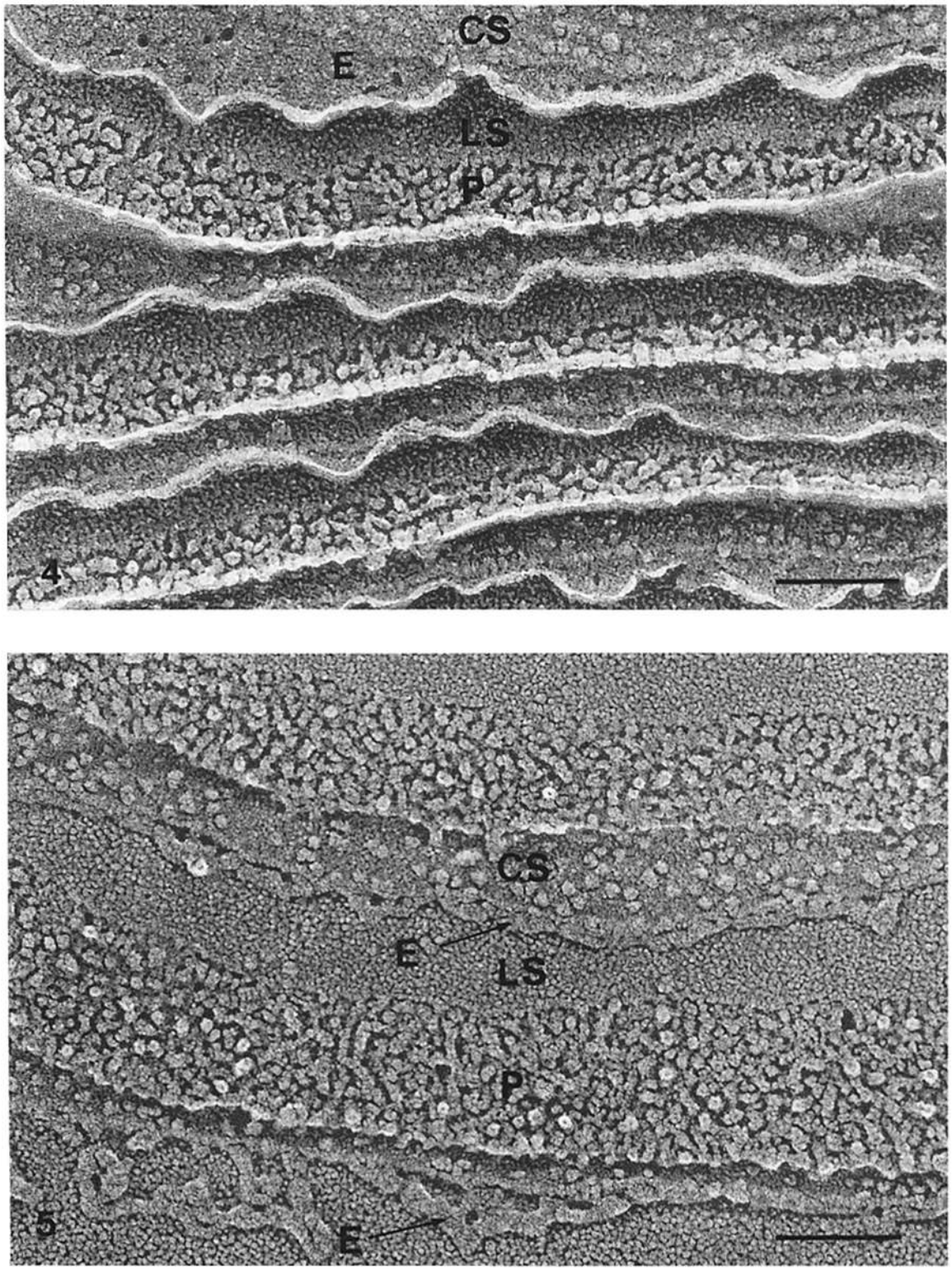

FIGURES 4 and 5 Fig. 4: Fragmented, swollen toad ROS treated as in Fig. 2 with brief etching (30 s at −95°C) followed by rotary Pt/C shadowing at an angle of 24°. The P face "cobblestones" appear cylindrical after rotary shadowing and the CS large particles look somewhat flattened. However, low angle rotary shadowing accentuates the random 6 nm bumps on the luminal surface (*LS*). Again note the pits present on the E fracture face after brief etching. Bar, 0.1 μm. × 200,000. Fig. 5: Deep-etched (3 min at −95°C) fragmented, swollen toad ROS, rotary shadowed as in Fig. 4. After 3 min of etching, large expanses of luminal membrane surface are visible due to an apparent break up of the overlying E fracture face. The fine 6-nm granularity is obvious on all regions of the LS disk membrane. Bar, 0.1 μm. × 200,000.

(18). The photoreceptor surface of the retina came in contact with a liquid helium cooled copper block (4°K), freezing the tips of the outer segments within ~1 ms at a rate exceeding 20,000°C/s (18). In the experiments using isolated disk membranes, a drop of the ROS fragment suspension was placed on a cushion of lung mounted on the freezing stage and excess solution was drawn off with filter paper immediately before freezing.

Freeze-fracture and -Etching

Frozen samples were kept under liquid nitrogen until transfer to the stage of a Balzers 301 freeze-fracture device (Balzers, Nashua, NH). The surface of the sample was gently scraped with a razor blade mounted in the freezing microtome to fracture the sample within the top 10 μm, the typical zone of good freezing. The vacuum was better than 2×10^{-6} torr and the tissue temperature was −110°C. The samples were etched at −95°C for various time intervals (30–180 s) as noted in the text. Some samples were unidirectionally shadowed at an angle of 45° with a 2-nm layer of platinum/carbon (Pt/C deposited to 210 Hz on a quartz crystal monitor). Others were rotary shadowed (28) with the Pt/C source mounted at an angle of 24°. (Pt/C was deposited to 195 Hz on the monitor.) For all samples the Pt/C source was an electron beam gun operated at 2,050-V and 70-μA beam current. All samples received 5 s of evaporated carbon by rotary deposition from a standard resistance source. Replicated tissue was cleaned in Purex bleach and transferred to 75 mesh formvar- and carbon-coated copper grids.

Microscopy and Measurement

Replicas were observed with either a JEOL 100C or a Philips 400 electron microscope at 80 kv or 100 kv. Photographic negatives were contact-reversed and all prints in this paper are negative images (platinum is white and shadows are black).

Particle sizes were measured from negatives with the aid of a dissecting microscope using a vernier eyepiece. Particle densities and sizes were also measured from the negatives and were measured only on areas of membrane which appeared flat, as judged by complete symmetry of shadows in the images of rotary shadowed samples.

A histogram of size distribution was made for the large irregularly shaped CS particles using the smallest measured dimension of each particle in rotary shadowed replicas. The size is reported as mean plus or minus standard deviation. A similar histogram was made for the large salt particles appearing in the Ringer's solution and the data is similarly reported. An attempt was also made to quantify the relative concentrations of 8–12 nm particles on the disk rim vs. the body of the disk. Particles (8–12 nm) were counted on a line drawn along the center of each disk rim (28 disks). All lines were longer than 0.2 μm. All particles <12 nm in diameter touching one of these lines were counted. Identical lines were constructed on the adjacent nonrim area of the same disks (where possible) and particles were similarly counted. The two samples, rim and nonrim, were tested for a significant difference in mean number of particles per unit length using Student's *t* test (44).

RESULTS

Comparison of Freeze-fracture and Deep-etching

The structure of the vertebrate rod photoreceptor outer segment is remarkably simple. When viewed in thin sections, the outer segment appears as a stack of 1,000 or more flattened vesicles or disks oriented perpendicular to the long axis of the cell and all contained by a single plasma membrane. Conventional freeze-fracture techniques have added to this perspective, information on the way the proteins are organized within the disk membrane. Again, the arrangement seems quite simple with stacks of hundreds of alternating particle-rich (P) and smooth (E) fracture faces (see reference 31 for review).

A typical freeze-fracture image of ROS quick frozen disks isolated from a *Bufo* retina is seen in Fig. 1. The only difference between this image and that of conventionally fixed, glycerinated, and slowly frozen retinas is a greater irregularity in the size and distribution of the particles found on the P fracture face of the rapidly frozen disk membranes. This irregularity in unfixed samples has also been observed in the P face of other rapidly frozen membranes (19) and it is attributed to the greater plasticity of unfixed membrane proteins.

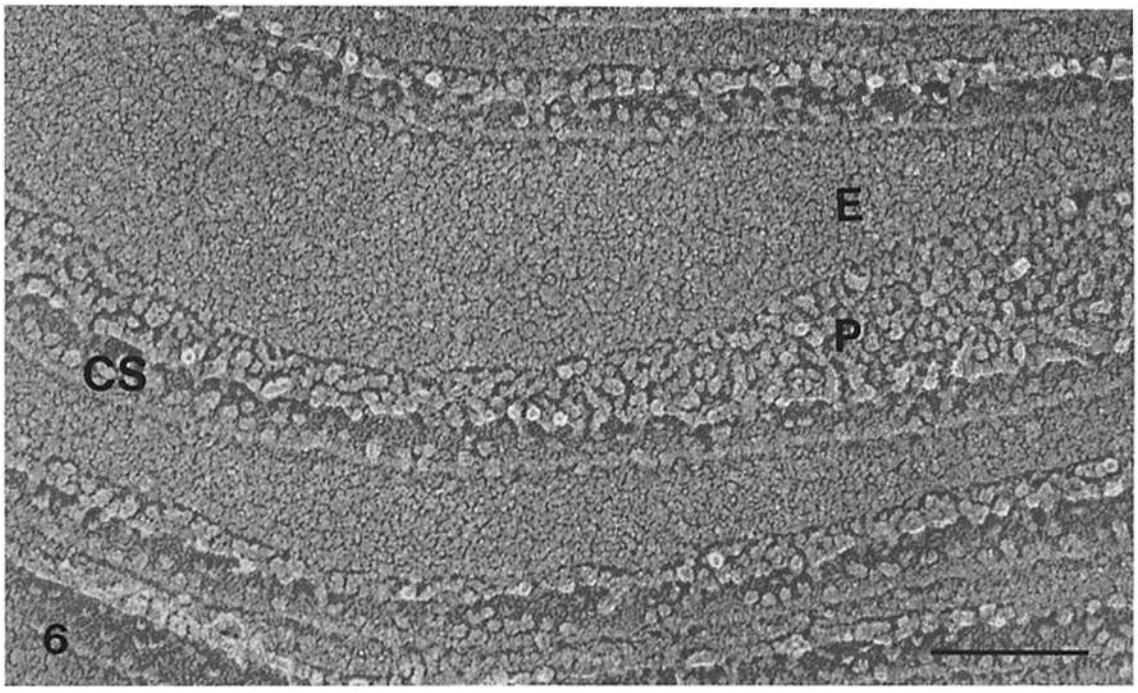

FIGURE 6 Disk membranes in a rapidly frozen ROS from intact toad retina. This ROS was etched for 3 min at −95°C after freeze-fracture and then rotary-shadowed at an angle of 24° with Pt/C. The smooth E fracture face and roughly particled P face are similar to those in rotary shadowed fragmented ROS (Figs. 4 and 5). A narrow band of CS interposed between P and E faces of adjacent disks has been exposed by etching. However, due to the very narrow intradisk space, not even a small area of luminal surface is visible between P and E faces of a single disk. Unfortunately, the E fracture face in intact retina does not break up upon etching to expose the underlying luminal membrane surface. Bar, 0.1 μm. × 210,000.

The disks shown in Fig. 1 were obtained from fragmented outer segments that had been hypotonically swollen during preparation. Thus they display relatively large spaces between the fracture faces which are not present in unperturbed whole retinas. The experimental advantage of the swollen ROS samples was that it permitted exposure of two additional faces after brief etching. For example, etching for 30 s at −95°C after fracture exposes two new surfaces in addition to the standard P and E fracture faces (Fig. 2). One is immediately adjacent to the P fracture face and possesses a very fine granular texture. This surface is separated by a distinct gap from the overlying E fracture face. Adjacent to the E face is another surface which appears to be covered by a scattering of larger bumps. Reference to Fig. 3 will explain the faces exposed by such etching. The finely granular face adjacent to the P fracture face represents the true inner surface of the disk, which we will hereafter term the luminal surface (LS). The other more roughly particled face represents the true outer surface of the disc, which is normally surrounded by the ROS cytoplasm. Hence we shall term it the CS of the disk membrane. This identification of intradisk and CSs can be confirmed by tracing around the lateral edges of the two disks displayed in Fig. 2.

LS of the Disk Membrane

The fine granular texture of the LS of the disk was only occasionally seen in samples that were unidirectionally shadowed at 45°, and only when the disk happened to be steeply tilted relative to the platinum source. The texture is much more obvious in samples that are rotary-replicated with the platinum gun mounted at 24°, such as that shown in Fig. 4. This figure displays a portion of a swollen ROS that was etched for 30 s after freeze-fracture, as was the sample in Fig. 2. Rotary-replication creates a circular or cylindrical halo around the large particles normally found on the P fracture faces, and also accentuates the subtle texture on the LS of the disk to a striking extent. This is most readily apparent in Fig. 5, which displays a similar preparation that was deep-etched at −95°C for 3 min rather than 30 s.

Surprisingly, prolonging the etching eventually causes the E fracture face to completely disappear. We found that this effect is progressive in swollen ROS. 30 s of etching made the E face look pitted. These pits enlarged to distinct holes by 90 s, and by 3 min of etching the holes became confluent, leaving behind nothing but an irregular network of raised material. Apparently, such progressive destruction of the E face is due to the rapid egress of water from the disk interior during etching. Water sublimating out of the disk interior must have blown through the E face and left a cavity underneath which further weakened this face. Such a mechanism has been proposed before by others (7). The same does not happen to the P

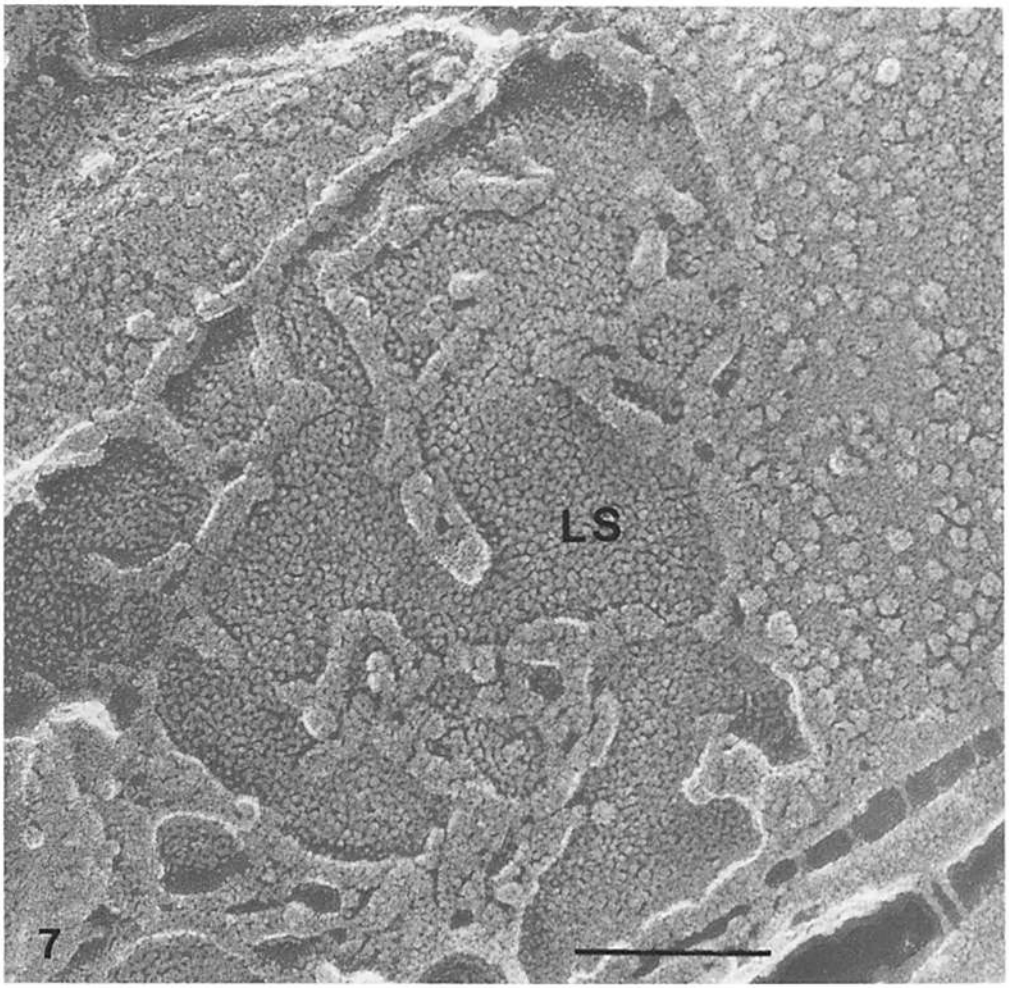

FIGURE 7 High magnification view of the LS of a disk membrane from fragmented toad ROS. Membranes were treated as in Fig. 5. A 6 nm granularity of ~30,000/μm^2 is seen on the LS. Fragments of broken up overlying E fracture face have been deposited onto the LS and on the adjacent cytoplasmic surface of this disk the 8–12 nm large particles are visible. Bar, 0.1 μm. × 260,000.

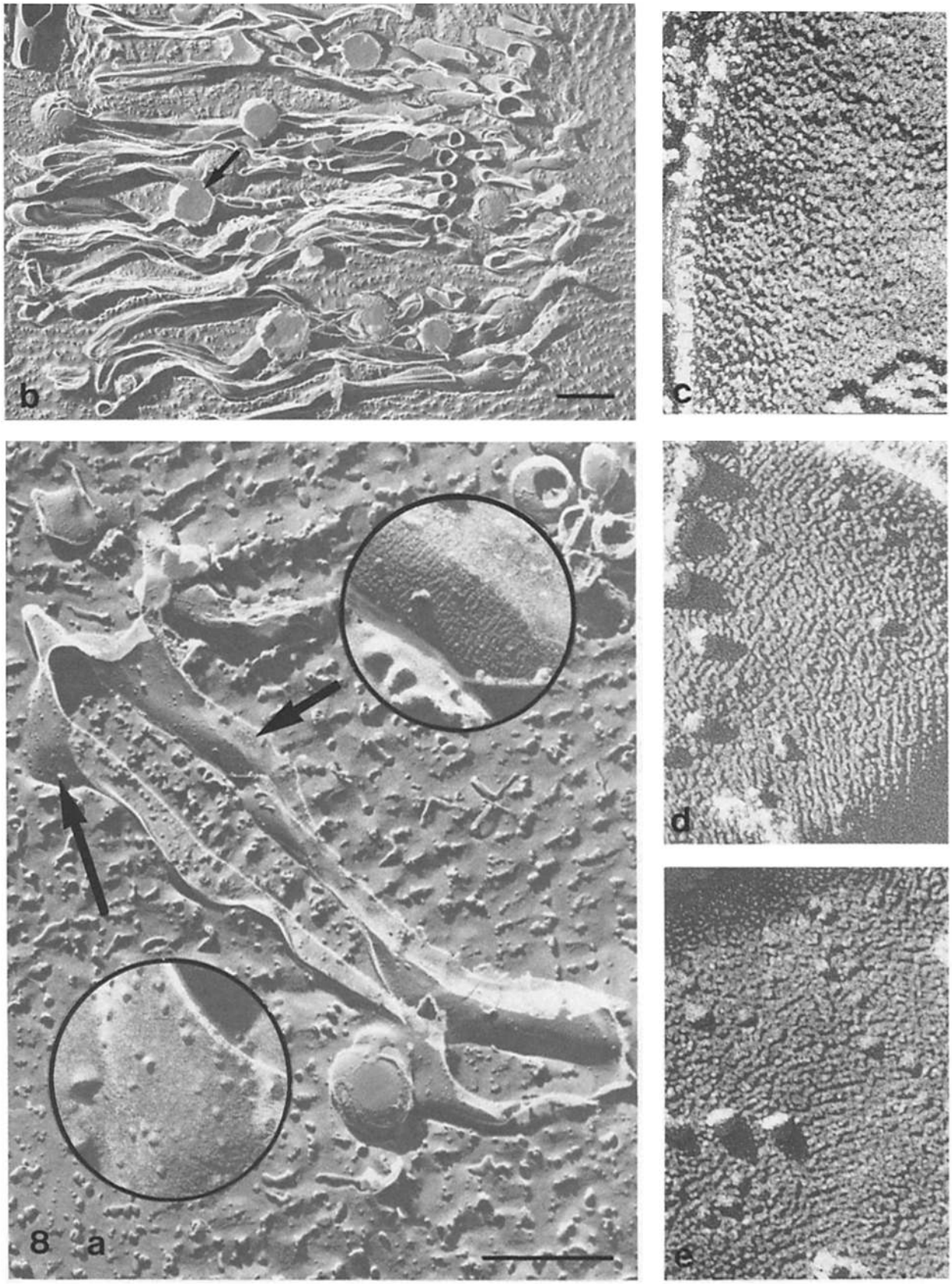

FIGURE 8 Disk membranes from fragmented toad ROS treated with phospholipase C (*a*, *b*, *d*, and *e*) and untreated control membranes (*c*). All membranes have been rapidly frozen, fractured at −110°C, etched for 3 min at −95°C, and unidirectionally shadowed at a 45° angle. Main figure shows part of a single disk membrane taken from a region like that in *b*. Prolonged digestion of disk membranes with phospholipase C has resulted in the formation of many lipid droplets (arrow, *b*) which contain the fatty acid residue of digested disk membrane lipids. As before, (Figs. 1, 2, and 4–7) high magnification views of the cytoplasmic surface (*lower inset*) show no 6-nm texture. However, a high magnification view of the lipid-depleted luminal surface (*upper inset*) of digested disks shows rowlike arrays of small particles. A direct comparison of the luminal surface from undigested control membranes (*c*) with phospholipase C digested membranes (*d* and *e*) emphasizes the apparent alteration in packing of 6-nm bumps after prolonged phospholipase C digestion. Bars, 0.5 μm. (*c*–*e*) × 300,000. *Insets*, × 158,000.

fracture face, possibly because it is thicker and more heavily loaded with protein.

The progressive destruction of the E fracture face upon deep-etching does not occur in intact retinas where the two membranes of a single disk are very closely apposed. In deep-etched intact retina, the LS of the disk is never exposed because it is always completely covered by the overlying E fracture face. The deep-etched intact retina in Fig. 6 shows both P and E fracture faces and the single cytoplasmic true surface which can be readily identified by comparison with the fragmented ROS in Figs. 4 and 5. Note, however, that the finely textured LS of the disk does not appear.

In any case, this destruction of the E fracture face in fragmented ROS is particularly fortuitous because it exposes large expanses of the LS of the disk which would otherwise have been obscured by overhanging ledges of the E fracture face. Reference to Fig. 3 will explain this point. Close inspection of the LSs in Fig. 5 and the one portrayed at higher magnification in Fig. 7 illustrate that they have a rough texture distinctly different from the background granularity of the replica, which is unfortunately also very coarse after rotary platinum deposition. Background granularity typically limits the resolution of platinum replicas to around 3–4 nm, but the rough texture on the LSs of disks is substantially larger than this. It appears in many places to be composed of a collection of ~6-nm bumps that are packed together at a near-confluent density of some 30,000/μm^2. An accurate size for individual bumps is difficult to estimate for such small, closely packed particles. The thickness of the Pt film and the shielding of each bump from the Pt source by other bumps probably contribute significantly to the

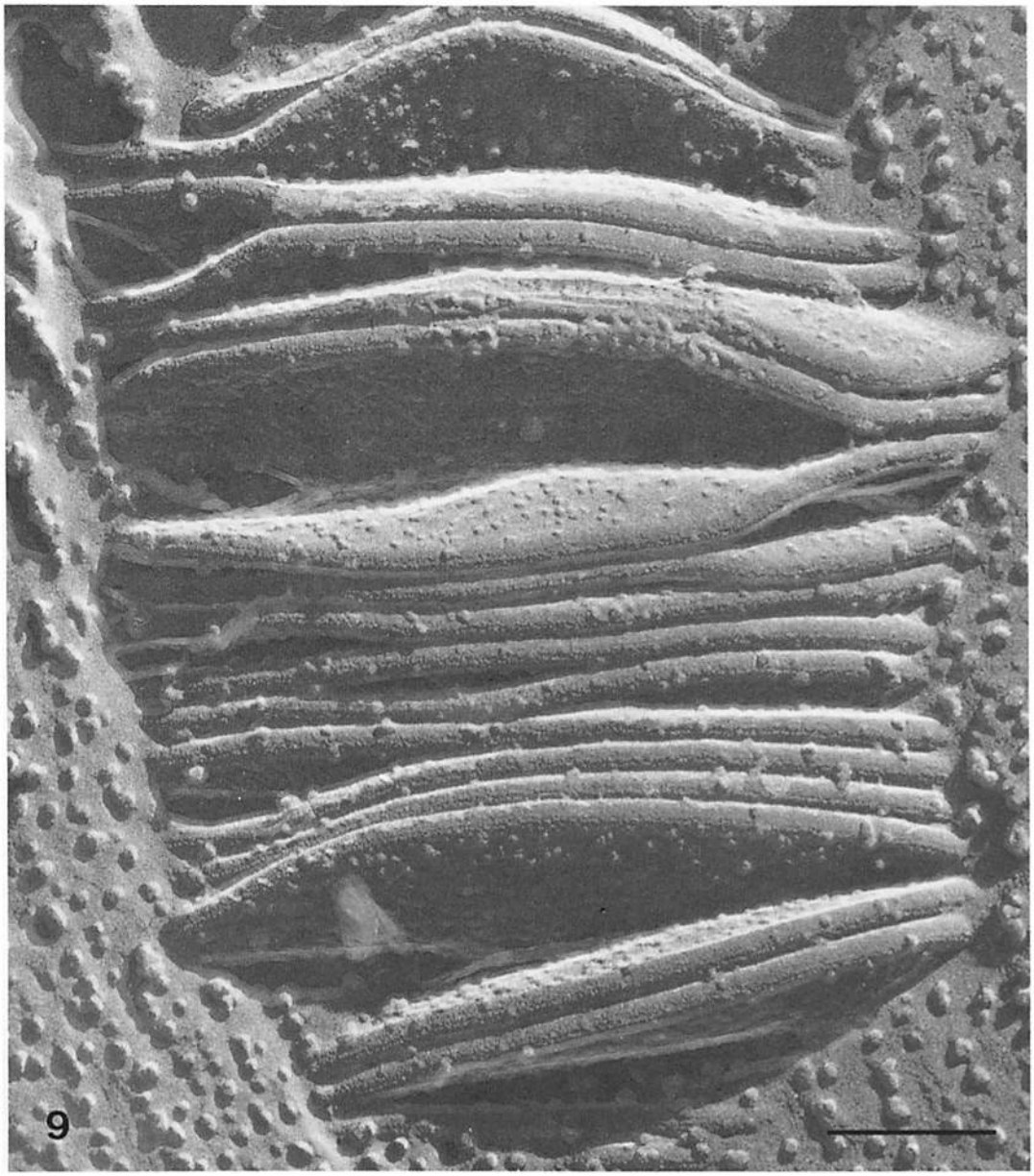

FIGURE 9 Stack of unfractured disks from a fragmented, swollen toad ROS which was rapidly frozen, fractured at −110°C, etched for 3 min at −95°C, and unidirectionally shadowed at an angle of 45°. The plasma membrane has been largely stripped away so that the fracture plane just grazes the disks. 8–12 nm particles are scattered across all interdisk (cytoplasmic) surfaces, but are not present at the disk rims. Larger background lumps are etched salts from the Ringer's solution in which this ROS was frozen. Bar, 0.1 μm. × 138,000.

image. However, assuming a close-packed configuration, 6 nm is an upper limit for the diameter of the underlying membrane feature. This size and the concentration of these bumps would suggest that they arise from protrusions of individual rhodopsin molecules into the lumen of the disk. The bumps much more faithfully reflect the size and packing of rhodopsin than do the intramembrane particles seen on the P fracture face of this membrane, which are much too large and irregular and present in much too low a concentration to be individual rhodopsins. The appearance and distribution of the intramembrane particles seen in freeze-fracture have always been difficult to relate to the biochemical composition of the disk membrane. However, based on these views of the disk lumen, we favor the idea that the intramembrane particles represent aggregates of many rhodopsins which collapse together when the luminal monolayer of phospholipids is fractured away from them during freeze-fracture.

A further indication that this is the correct interpretation of the intradisk texture comes from experiments using phospholipase C. As reported by Olive et al. (32) and van Brugel et al. (47), exhaustive digestion of disk membranes with phospholipase C causes 90% of the disk phospholipid to be segregated into large droplets. This is seen in Fig. 8 *b*. In addition, we found that the concentration of rhodopsin in the remainder of the disk perforce increases, leading to an unusual change in rhodopsin packing. Fig. 8 *a*, *d*, and *e* show areas of rowlike arrays of small particles on the intradisk surface. Thus, the packing of rhodopsin and the small 6-nm particles are simultaneously perturbed by phospholipase C digestion.

CS of the Disk Membrane

A return to Figs. 4 and 5 permits close inspection of the other true membrane surface exposed by deep-etching, namely the CS. It displays a collection of large particles scattered randomly across its surface. These are quite irregular in shape, though a size frequency histogram of the particles' minimum dimension (data not shown) is unimodal with a mean size of 10 nm and a range of 8–12 nm (10.1 ± 1.1 nm). Their concentration is ~2,700/μm^2 in fragmented ROS, only $\frac{1}{11}$ of that of the fine 6-nm bumps seen on the luminal surface. This concentration was similar in all three vertebrate species examined: toad, rat, and cattle.

The best preparations for viewing this CS were again the hypotonically treated retinas, which often released ROSs in which the outer plasma membrane was stripped away but in which disks were still stacked together. Very deep-etching of such samples often exposed stacks of disks such as those shown in Fig. 9. Here, unlike the previous figures, there can be no question about the interpretation of fracture and etching planes. Exposed is the lateral edge of a stack of flattened disks which have begun to separate from each other in certain regions. It is readily apparent that the large particles which characterize the true CS are present on both sides of each disk.

The reader will note that larger particles (smallest dimension = 17.2 nm ± 4.8 nm) are also found on the ice table which surrounds these stacks of disks. This is the characteristic image of nonvolatile salts that are left behind during deep-etching; in this case, from the one-tenth isoosmotic Ringer's solution in

FIGURE 10 High magnification view of disk rims from fragmented, swollen toad ROS treated as in Fig. 9, and rotary-shadowed at an angle of 24°. Filamentlike connections between disk rims appear to stretch before breaking. No residue of broken filaments is deposited on the disk rims in areas where the rims have become separated. Bar, 0.1 μm. × 230,000.

which this preparation was suspended. A size frequency histogram for the minimum dimension of these salt particles shows no single average (data not shown) with peaks at 12, 15, and 20 nm and a range from 10 to 40 nm. This is in contrast to the unimodal distribution of 8–12 nm particles found on the disk surface. Further, the significant difference ($P < 0.005$; Fisher's F test [44]) between the variances of the two populations (salt and membrane bound particles) makes it unlikely that the particles on the CS of the disk represent smaller crystals of nonvolatile salts deposited onto the membrane. In addition, further dilution of the Ringer's reduced the concentration of these background dots, but did not alter the appearance of the smaller particles we are describing on the membrane. Conversely, salt added back to membranes purposely stripped of protein did not restore the CS particles. Thus we do not think that the membrane particles are a salt contaminant left behind during deep-etching. Furthermore, we do not think they are simply adsorbed cytoplasmic proteins, because not even overnight washing of the isolated disks would remove them. Finally, the most compelling reason for believing that these particles are a bona fide component of the disk membrane is that their distribution is nonrandom. The concentration of particles along disk rims was found to differ significantly ($P < 0.001$; Student's t test [44]) from the concentration in nonrim areas. There were approximately five times fewer particles at the very edges of the disks, where a separate rim structure can be seen.

Structures on the Disk Rims

One differentiation that is found around the rim of every disk might have been predicted from the fact that disks tend to hold together in stacks even after the plasma membrane has been removed (9). It consists of many thin filaments which connect adjacent disks as seen in Fig. 10. These filaments are spaced regularly about every 14 nm in intact retina (Fig. 11), and they are set in from the disk edge by ~15 nm. In contrast, very few and sparsely scattered connections are observed between nonrim areas of disks. As seen at high magnification in Fig. 10, when isolated disks begin to separate, these filaments appear to be able to stretch up to 30 nm before breaking. Once separation is complete, however, their remnants cannot be discerned on the membrane surface. Usukura and Yamada (46) have recently reported the observation of similar filaments using thin-section freeze substitution.

Similar filaments are often found bridging the deep clefts or incisures in multilobulated amphibian disks. Those filaments seen in Fig. 12 connect different parts of the same disk rim across incisures.

Other filamentlike structures appear to connect disks to the plasma membrane in both amphibian and mammalian rods. In toads, these plasma membrane connections are very short (<10 nm) and are irregularly spaced, but in rat and cattle rods they are capable of stretching up to 30 nm and are often branched. This irregular and branched appearance, as seen in Fig. 13, suggests that the disk to plasma membrane "filaments" may be chemically different from their more regular unbranched counterparts associated strictly with disk rims. In addition, these plasma membrane to disk connections persist even after the plasma membrane continuity and disk stacking have been severely disrupted. As suggested by the thin-section micrographs of Cohen (9; see Cohen's Fig. 20) and confirmed in Fig. 14 by deep-etching, the persistent association of disrupted disks with fragments of plasma membrane may be mediated by these filamentlike entities.

DISCUSSION

Here we present views of ROS disk membranes which are significantly different from any formerly obtained by freeze-fracture. The added step of deep-etching after freeze-fracture has exposed the true surfaces of disk membranes which show a distinct sidedness. A characteristic texture observed on the LS of the disk membrane is not present on its CS.

LS of the Disk Membrane

The fine texture on the LS of the disk has the proper size and packing dimensions to correspond to individual rhodopsin

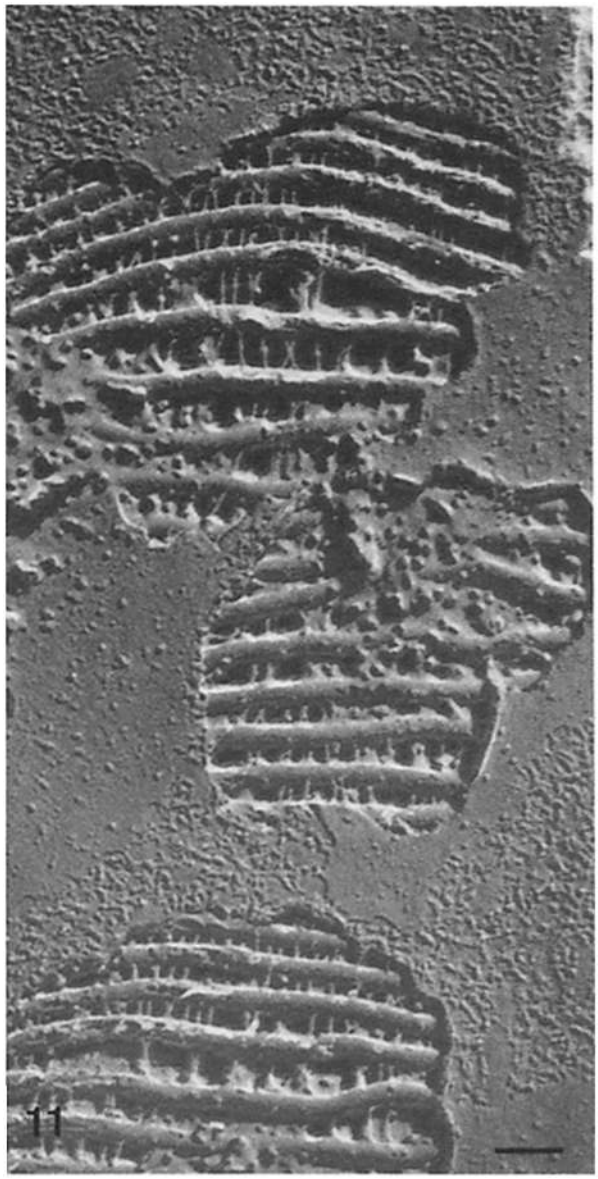

FIGURE 11 Disk rims from a ROS in intact toad retina, rapidly frozen, fractured at −110°C, etched for 3 min at −95°C, and unidirectionally shadowed at an angle of 45°. The ROS plasma membrane (readily identified by particle-free patches on the P fracture face) has been fractured away to expose disk rims after deep-etching. Disk-to-disk connections spaced about every 14 nm are seen between adjacent disk rims. Bar, 0.1 μm. × 96,000.

molecules. Proteolytic digestion and chemical labeling studies (21) have shown that rhodopsin spans the lipid bilayer and recent neutron diffraction results place the bulk of the rhodopsin mass within the hydrophobic core of the disk membrane (40). It is not known how much of the volume of rhodopsin is present at either surface of the disk membrane. Despite chemical evidence (21) for rhodopsin *exposure* at the CS, no substantial protrusion there has been resolved using x-ray or neutron scattering. The only information about the protrusion of rhodopsin above the membrane surface is that inferred from the two carbohydrate chains known to be covalently linked to rhodopsin (17), which penetrate into the intradisk space (2, 36). The dimensions of these carbohydrate moieties (each ~2–4 nm long and 4 nm in diameter, assuming a rigid chain perpendicular to the disk surface [11, 35, 37]) could account for the protrusions we see. Of course, it must be noted that the surface

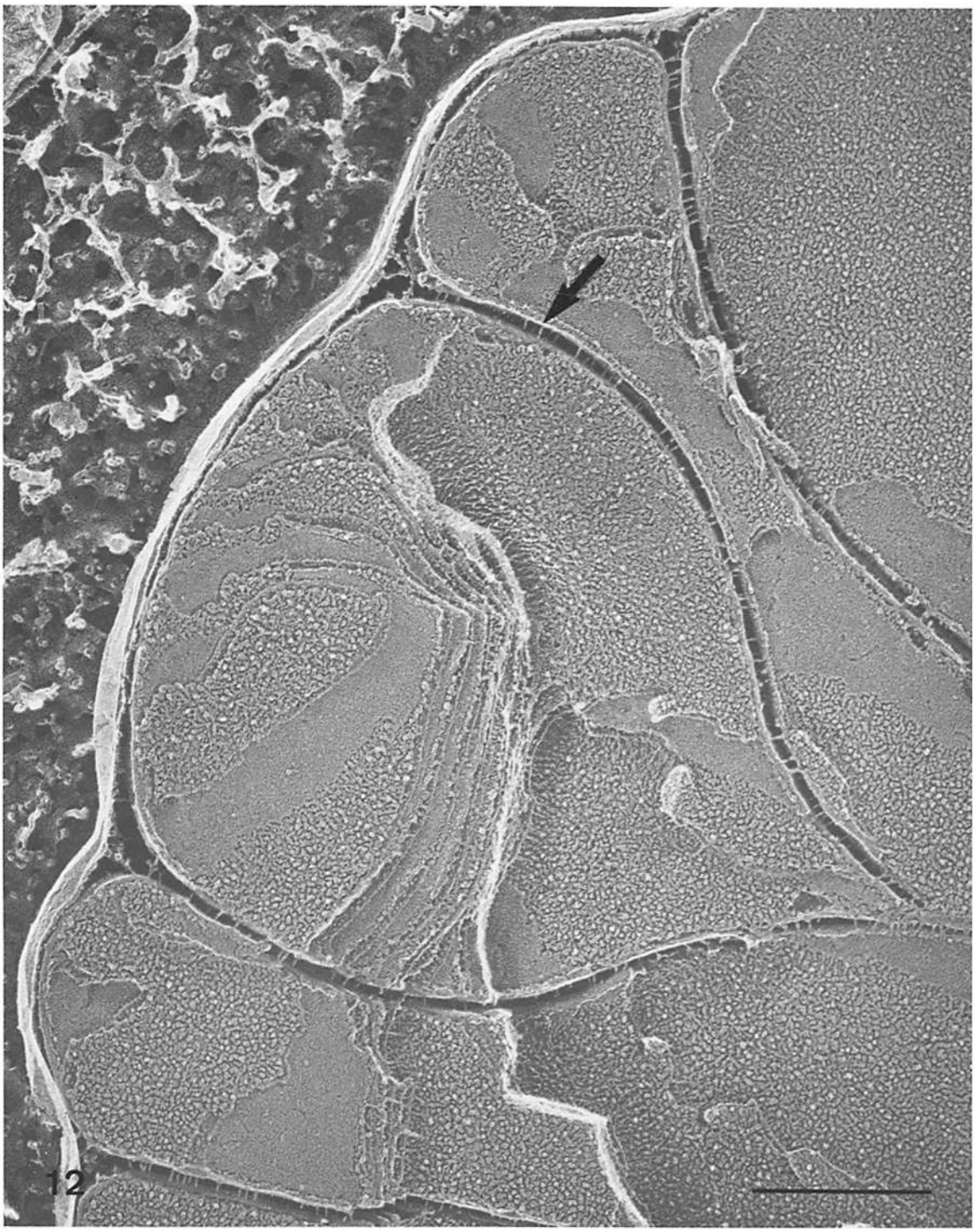

FIGURE 12 Cross-section fracture of a multilobulated disk from an intact toad retina, prepared as in Fig. 12; etched for 3 min at −95°C and rotary-shadowed at an angle of 24°. Short filamentlike connections bridge the deep clefts or incisures (arrow). Bar, 0.1 μm. × 70,000.

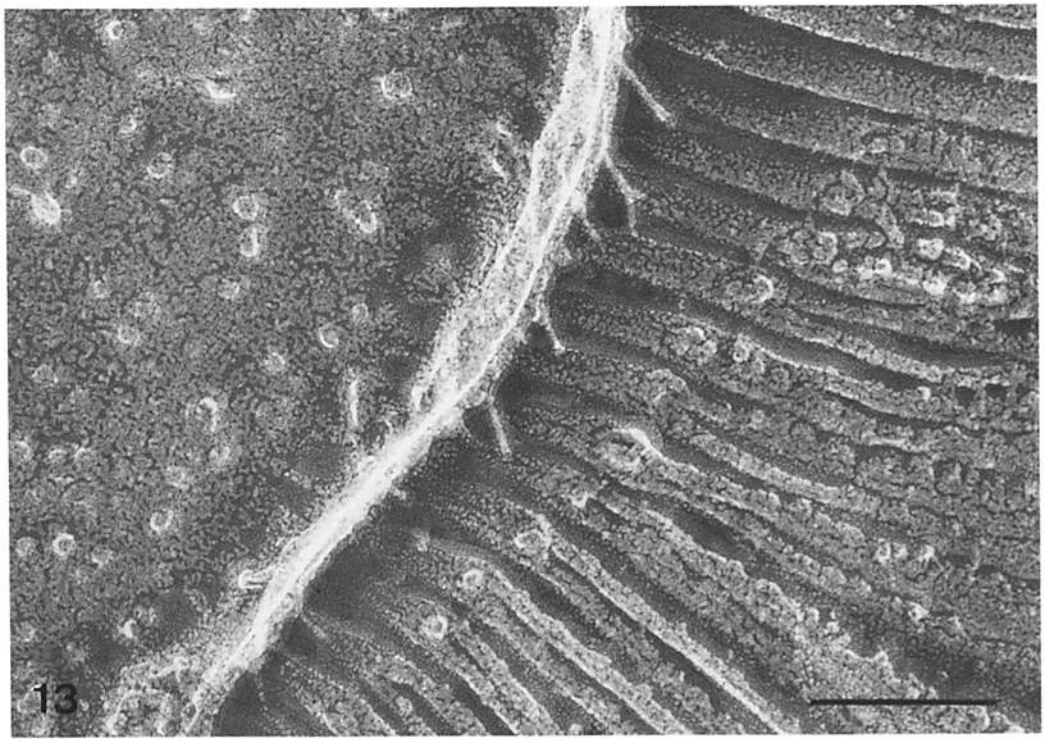

FIGURE 13 Fragmented, swollen ROS from *cattle* retina, rapidly frozen, fractured at −110°C, etched for 3 min at −95°C and rotary shadowed at an angle of 24°. Scattered, thin, branched connections appear to link disk rims with the adjacent plasma membrane. Bar, 0.1 μm. × 250,000.

texture in question is very close to the limit of resolution imposed by the granularity of our platinum replica (1). Indeed, the texture we see undoubtedly arises partly from chemical interactions of condensing platinum with the underlying structures in the membrane. Thus it may be primarily a "decoration" phenomenon, but since it is observed in no other membrane, it must reflect this membrane's underlying content of rhodopsin.

To confirm this assignment we used phospholipase C digestion of ROS membranes which is known to alter rhodopsin packing by segregating phospholipids into droplets. We found that phospholipase C also alters the luminal texture. Unfortunately, it is not possible to quantify the effects of phospholipase C on rhodopsin packing in a manner which would permit direct correlation with the observed change in surface texture. Thus we are currently pursuing other, less perturbing methods for altering rhodopsin concentration in the membrane.

CS of the Disk Membrane

The CS of the disk does not display the same fine texture as the LS. Instead, the CS exhibits large, irregularly shaped particles scattered across the disk surface. The size of the particles, their number, and the invariance of these values across a wide range of species suggests that they may represent some or all of the peripheral membrane-bound proteins known to localize to the cytoplasmic side of the disk. Those present in the largest amounts have been identified biochemically as a GTP-binding protein (4, 13, 15, 25) (also known as 80 K [3], light-activated GTPase [6], transducin [12], G-protein [4, 43]) and a light activated cGMP phosphodiesterase (PDE) (3, 29). The remainder of the disk proteins are present in smaller amounts. In the following paper we will describe work that permitted us to determine which of these proteins are represented by the large particles.

Further Differentiations at the Disk Rim

The rim of each disk is a distinct and separate domain. Falk and Fatt (10) first showed chemical differences between rims and lamellae of disks by a method which chemically destroyed lamellae leaving rims intact. Recently, Papermaster et al. (33) have shown that the protein composition of the rim area is different from the body of the disk. Here we have shown that membrane features such as the large particles are present everywhere on the CS but at lower concentration on the disk rim. The genesis of this rim differentiation is suggested in the model for disk formation proposed by Steinberg et al. (45), in which the rim is formed by a separate mechanism and from a separate part of the ciliary membrane region in the rod. However, the maintenance of such distinct domains in a membrane known to be highly fluid is more difficult to explain. Perhaps the maintenance of these domains is related to another aspect of rim structure. Two filamentlike specializations are associated exclusively with disk rims. One of these appears to connect the rims of adjacent disks within the stack, while the other connects different parts of the same disk rim across disk incisures. The molecular nature of these filaments is unknown. It is possible that the filaments could be the 290,000 dalton "rim protein" described by Papermaster et al. (33). The location of rim protein and filaments is similarly confined primarily to rims and incisures and the size expected of a protein filament 7-nm-by-14-nm would be in the range of 290,000 dalton. However, the total numbers of rim proteins and filaments match rather poorly. Biochemical estimates of the abundance of rim protein (1,000–3,000 molecules per disk [33]) do not fit well with our rough estimates of the number of rim filaments that appear to be present (this is 8,000 filaments per disk, if they are all regularly spaced every 14 nm as they are in the most ordered areas).

Regardless of their molecular composition, the rim specializations look as if they could play an obvious role in stabilizing

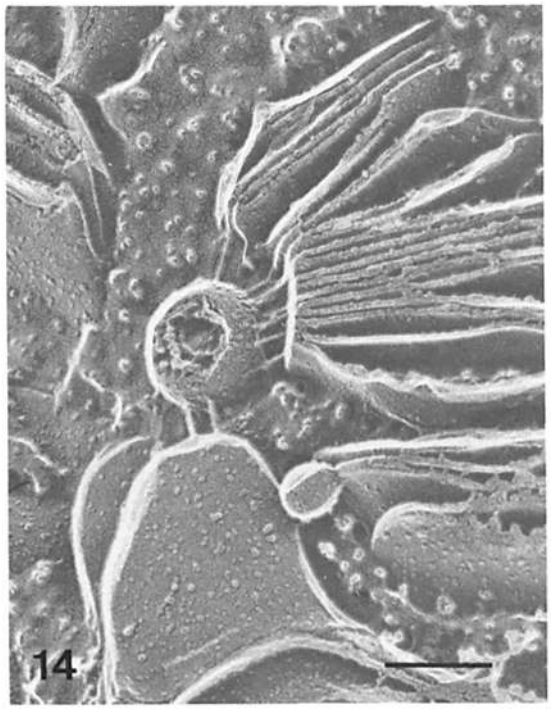

FIGURE 14 Cattle disks prepared by sucrose flotation, then washed free of sucrose before rapid-freezing. Disks were fractured at −110°C, etched for 3 min at −95° and rotary-shadowed at an angle of 45°. Cohen (9) has suggested that his similar thin section views represent disks which remain in close contact with a small piece of vesiculated plasma membrane. Not visible in Cohen's thin section micrographs, but exposed here by deep-etching are filamentlike connections which appear to mediate the attachment of disks to plasma membrane. Bar, 0.1 μm. × 140,000.

ROS architecture. Disks do hold together even in the absence of the plasma membrane, as Fig. 9 demonstrates so dramatically. This has been known for many years (9). In addition, disk incisures are somehow kept in precise register over the entire length of the ROS and the disks are spaced with almost crystalline regularity along the axis of the rod. It can be calculated (P. W. Meyer, personal communication) that without some restraining influence, Brownian movements of the disk would result in their rotating relative to each other ~90° in 4 h, resulting in rapid misalignment of disk incisures. This does not happen even over the entire lifetime of a disk (~40 d in the frog [50]). The rim filaments are clearly the most likely structure to prevent such disorganization.

In addition to the disk-to-disk connections, another type of contact seems to be made between the disks and the plasma membrane. The appearance of disk to plasma membrane filaments is distinct from rim filaments; they are less regularly spaced, somewhat longer than interdisk filaments and sometimes appear to be branched. Some previous observations put severe limits on their possible function. They cannot be the remnants of tubes which connect intradisk space with the external space of the rod. This is ruled out by the lanthanum and procion yellow penetration experiments of Cohen (8) and Laties and Liebman (26). In addition, the cable properties of the rod show that the plasma membrane is in electrical continuity with, at most, 30 open disks at the base of the outer segment (16). Nevertheless, the stubborn adherence of disks to plasma membrane when rods are disrupted (see Cohen [9] and Fig. 14) suggests that PM filaments may also serve a structural role in keeping the plasma membrane anchored in close proximity to the disk rim. Whether either of these filament types play an important role in phototransduction remains to be seen.

The authors would like to thank J. Korenbrot for many helpful discussions including the suggestion of the phospholipase experiments, for critically reading the manuscript, and generous support to D. J. Roof. Dr. Roof would like to thank L. Evans, F. McKeon, and N. Hirokawa for assistance in performing the initial experiments, M. Zimmerman for darkroom assistance, A. Dillon for drawing Fig. 3, and P. Meyer for critically reading the manuscript.

This work was supported by grants to J. E. Heuser from the U. S. Public Health Service (NS-11979) and the Muscular Dystrophy Association of America. D. J. Roof was supported by the Department of Biochemistry, University of California, San Francisco and by a grant to J. Korenbrot (EY-01586).

Received for publication 29 January 1982, and in revised form 3 June 1982.

REFERENCES

1. Abermann, R., M. M. Salpeter, and L. Bachmann. 1972. High resolution shadowing. *Principles and Techniques of Electron Microscopy.* 2:197–217.
2. Adams, A. J., R. L. Somer, and H. Shichi. 1979. Spatial arrangement of rhodopsin in the disk membrane as studied by enzymatic labeling. *Photochem. Photobiol.* 29:687–692.
3. Baehr, W., M. J. Devlin, and M. L. Applebury. 1979. Isolation and characterization of cGMP phosphodiesterase from bovine rod outer segments. *J. Biol. Chem.* 254:11669–11677.
4. Baehr, W., E. Morita, R. Swanson, and M. Applebury. 1982. Characterization of bovine rod outer segment G-protein. *J. Biol. Chem.* 257:6452–6460.
5. Bitensky, M. W., R. E. Gorman, and W. H. Miller. 1971. Adenyl cyclase as a link between photon capture and changes in membrane permeability of frog photoreceptors. *Proc. Natl. Acad. Sci. U. S. A.* 68:561–562.
6. Bitensky, M. W., G. L. Wheeler, B. Aloni, S. Vetury, and Y. Matuo. 1978. Light- and GTP-activated photoreceptor phosphodiesterase: regulation by a light-activated GTPase and identification of rhodopsin as the phosphodiesterase binding site. *Adv. Cyclic Nucleotide Res.* 9:553–572.
7. Chen, Y. S., and W. L. Hubbell. 1973. Temperature- and light-dependent structural changes in rhodopsin-lipid membranes. *Exp. Eye Res.* 17:517–532.
8. Cohen, A. I. 1970. Further studies on the question of the patency of the saccules in outer segments of vertebrate photoreceptors. *Vision Res.* 10: 445–453.
9. Cohen, A. I. 1971. Electron microscope observations on form changes in photoreceptor outer segments and their saccules in response to osmotic stress. *J. Cell Biol.* 48:547–565.
10. Falk, G., and P. Fatt. 1969. Distinctive properties of the lamellar and disk-edge structures of the rod outer segment. *J. Ultrastruct. Res.* 28: 41–60.
11. Fukuda, M. N., D. S. Papermaster, and P. A. Hargrave. 1979. Rhodopsin carbohydrate. *J. Biol. Chem.* 254:8201–8207.
12. Fung, B., J. B. Hurley, and L. Stryer. 1981. Flow of information in the light-triggered cyclic nucleotide cascade of vision. *Proc. Natl. Acad. Sci. U. S. A.* 78:152–156.
13. Fung, B., and L. Stryer. 1980. Photolyzed rhodopsin catalyzes exchange of GTP for bound GDP in retinal rod outer segments. *Proc. Natl. Acad. Sci. U. S. A.* 77:2500–2504.
14. Godchaux, W., and W. F. Zimmerman. 1979. Soluble proteins of intact bovine rod cell outer segments. *Exp. Eye Res.* 28:483–500.
15. Godchaux, W., and W. F. Zimmerman. 1979. Membrane-dependent guanine nucleotide binding and GTPase activities of soluble protein from bovine rod cell outer segments. *J. Biol. Chem.* 254:7874–7884.
16. Hagins, W. A., and H. Ruppel. 1971. Fast photoelectric effects and the properties of vertebrate photoreceptors as electric cables. *Fed. Proc.* 30:64–68.
17. Hargrave, P. A. 1977. The amino-terminal tryptic peptide of bovine rhodopsin. A glycopeptide containing two sites of oligosaccharide attachment. *Biochim. Biophys. Acta.* 492:83–94.
18. Heuser, J. E., T. S. Reese, M. J. Dennis, Y. Jan, L. Jan, and L. Evans. 1979. Synaptic vesicle exocytosis captured by quick-freezing and correlated with quantal transmitter release. *J. Cell Biol.* 81:275–300.
19. Heuser, J. E., and S. R. Salpeter. 1979. Organization of acetylcholine receptors in quick-frozen, deep-etched, and rotary-replicated *Tropedo* postsynaptic membrane. *J. Cell Biol.* 82:150–173.
20. Hubbell, W. L., and M. D. Bownds. 1979. Visual transduction in vertebrate photoreceptors. *Annu. Rev. Neurosci.* 2:17–34.
21. Hubbell, W. L., and B. Fung. 1979. The structure and chemistry of rhodopsin: relationship to models of function. *In* Membrane Transduction Mechanisms. R. A. Cone and J. Dowling, editors. Raven, New York. 17–25.
22. Korenbrot, J. I., D. T. Brown, and R. A. Cone. 1973. Membrane characteristics and osmotic behavior of isolated rod outer segments. *J. Cell Biol.* 56:389–398.
23. Kuhn, H. 1980. Light- and GTP-regulated interaction of GTPase and other proteins with bovine photoreceptor membranes. *Nature (Lond.).* 283:587–589.
24. Kuhn, H. 1981. Interactions of rod cell proteins with the disk membrane: influence of light, ionic strength, and nucleotides. *Curr. Top. Membr. Transp.* 15:171–201.
25. Kuhn, H., and P. A. Hargrave. 1981. Light-induced binding of guanosine triphosphatase to bovine photoreceptor membranes: effect of limited proteolysis of the membranes. *Biochemistry.* 20:2410–2417.
26. Laties, A. M., and P. A. Liebman. 1970. Cones of living amphibian eye: selective staining. *Science (Wash. D. C.)* 168:1475–1476.
27. Liebman, P. A., and E. N. Pugh. 1979. The control of phosphodiesterase in rod disk membranes: kinetics, possible mechanisms and significance for vision. *Vision Res.* 19:375–380.
28. Margaritis, L. H., A. Elgsaeter, and D. Branton. 1977. Rotary replication for freeze-

etching. *J. Cell. Biol.* 72:47–56.
29. Miki, N., J. M. Baraban, J. J. Keirns, J. J. Boyce, and M. W. Bitensky. 1975. Purification and properties of light activated cyclic nucleotide phosphodiesterase in rod outer segments. *J. Biol. Chem.* 250:6320–6327.
30. Molday, R. S., and L. L. Molday. 1979. Identification and characterization of multiple forms of rhodopsin and minor proteins in frog and bovine rod outer segment disk membranes. *J. Biol. Chem.* 254:4653–4660.
31. Olive, J. 1980. The structural organization of mammalian retinal disc membranes. *Int. Rev. Cytol.* 64:107–169.
32. Olive, J., E. L. Benedetti, J. G. M. Van Breugel, P. J. M. Daemen, and S. L. Bonting. 1978. Biochemical aspects of the visual process. XXXVII. Evidence for lateral aggregation of rhodopsin molecules in phospholipase C-treated bovine photoreceptor membranes. *Biochim. Biophys. Acta.* 509:129–135.
33. Papermaster, D. S., B. G. Schneider, M. A. Zorn, and J. P. Kraehenbuhl. 1978. Immunocytochemical localization of a large intrinsic membrane protein to the incisures and margins of frog rod outer segment disks. *J. Cell Biol.* 78:415–425.
34. Pober, J. S., and M. W. Bitensky. 1979. Light-regulated enzymes of vertebrate retinal rods. *Adv. Cyclic Nucleotide Res.* 11:265–301.
35. Rao, V. S. R. 1975. Average dimensions of a monosaccharide unit. *In* Handbook of Biochemistry and Molecular Biology: Lipids, Carbohydrates, and Steroids. 3rd edition. G. D. Fasman, editor. CRC Press, Cleveland, Ohio. 472–473.
36. Rohlich, P. 1976. Photoreceptor membrane carbohydrate on the intradiscal surface of retinal rod disks. *Nature (Lond.).* 263:789–791.
37. Romhanyi, G., and L. Molnar. 1974. Optical polarization indicates linear arrangement of rhodopsin oligosaccharide chain in rod disk membranes of frog retina. *Nature (Lond.).* 249:486–488.
38. Roof, D. J., J. I. Korenbrot, and J. E. Heuser. 1980. Surfaces of rod photoreceptor disk membranes, exposed by deep etching. *J. Cell Biol.* 87(2, Pt. 2):1542*a* (Abstr.).
39. Roof, D., J. Korenbrot, and J. Heuser. 1981. Surfaces of rod photoreceptor disk membranes. *Soc. Neurosci. Abstr.* 7:729 (Abstr.).
40. Saibil, H., M. Chabre, and D. Worcester. 1976. Neutron diffraction studies of retinal rod outer segment membranes. *Nature (Lond.).* 262:266–270.
41. Shichi, H., and R. L. Somers. 1980. Distribution of enzymes involved in nucleotide metabolism in the disk and other rod membranes. *Photochem. Photobiol.* 32:491–495.
42. Shinozawa, T., and M. W. Bitensky. 1980. Co-operation of peripheral and integral membrane proteins in the light dependent activation of rod GTPase and phosphodiesterase. *Photochem. Photobiol.* 32:497–502.
43. Shinozawa, T., S. Uchida, E. Martin, D. Cafiso, W. Hubbell, and M. Bitensky. 1980. Additional component required for activity and reconstitution of light-activated vertebrate photoreceptor GTPase. *Proc. Natl. Acad. Sci. U. S. A.* 77:1408–1411.
44. Snedecor, G. W., and W. G. Cochran. 1967. Statistical Methods. Iowa State University Press, Ames, Iowa.
45. Steinberg, R. H., S. K. Fisher, and D. H. Anderson. 1980. Disk morphogenesis in vertebrate photoreceptors. *J. Comp. Neurol.* 190:501–518.
46. Usukura, J., and E. Yamada. 1981. Molecular organization of the rod outer segment. A deep-etching study with rapid freezing using unfixed frog retina. *Biomedical Research.* 2:177–193.
47. Van Breugel, P. J. G. M., P. H. M. Geurts, P. J. M. Daemen, and S. L. Bonting. 1978. Biochemical aspects of the visual process. XXXVIII. Effects of lateral aggregation on rhodopsin in phospholipase C-treated photoreceptor membranes. *Biochim. Biophys. Acta.* 509:136–147.
48. Woodruff, M. L., and M. D. Bownds. 1979. Amplitude, kinetics and reversibility of a light-induced decrease in guanosine 3′,5′-cyclic monophosphate in frog photoreceptor membranes. *J. Gen. Physiol.* 73:629–653.
49. Yoshikami, S., and W. A. Hagins. 1971. Light, calcium, and the photocurrent of rods and cones. *Abstracts of the Biophysical Society Meeting.* 47*a* (Abstr.).
50. Young, R. W., and B. Droz. 1968. The renewal of protein in retinal rods and cones. *J. Cell Biol.* 30:169–184.